Electrostatic hexapole state-selection of the asymmetric-top molecule propylene oxide: Rotational and orientational distributions

ARTICLE *in* CHEMICAL PHYSICS · MAY 2012

Impact Factor: 1.65 · DOI: 10.1016/j.chemphys.2011.11.020

5 AUTHORS, INCLUDING:

Federico Palazzetti
Università degli Studi di Perugia
35 PUBLICATIONS **340** CITATIONS
SEE PROFILE

Vincenzo Aquilanti
Università degli Studi di Perugia
315 PUBLICATIONS **6,454** CITATIONS
SEE PROFILE

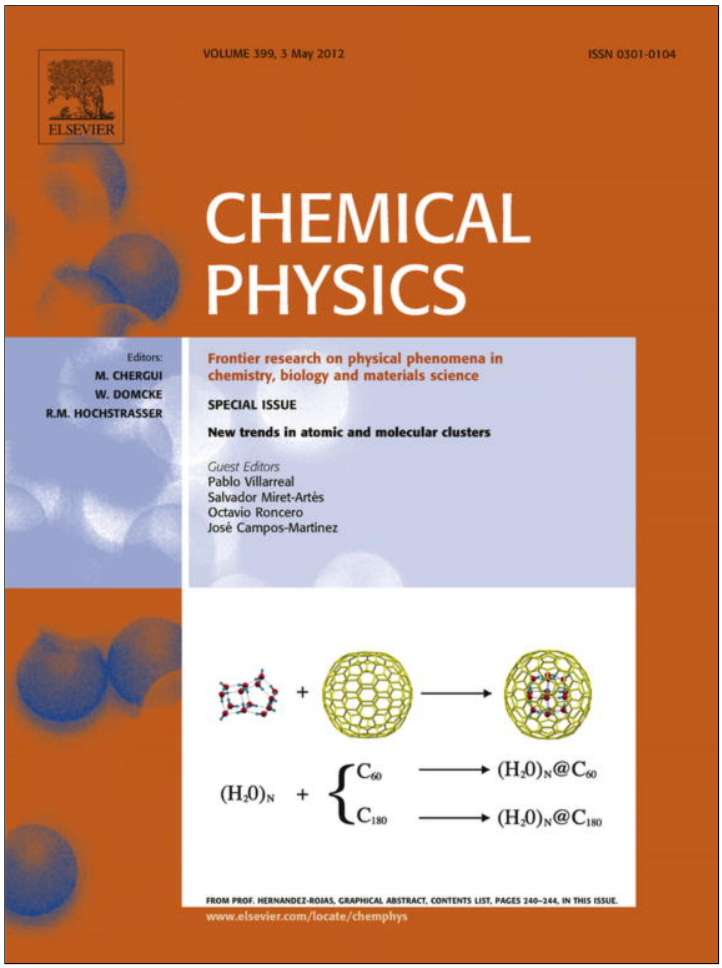

Chemical Physics 399 (2012) 180–192

Contents lists available at SciVerse ScienceDirect

Chemical Physics

journal homepage: www.elsevier.com/locate/chemphys

Electrostatic hexapole state-selection of the asymmetric-top molecule propylene oxide: Rotational and orientational distributions ☆

Dock-Chil Che [a], Keita Kanda [a,*], Federico Palazzetti [b,*], Vincenzo Aquilanti [b], Toshio Kasai [a,c]

[a] Osaka University, Department of Chemistry, Graduate School of Science Toyonaka, Osaka 560-0043, Japan
[b] Università di Perugia, Dipartimento di Chimica, 06123 Perugia, Italy
[c] National Taiwan University, Department of Chemistry, No. 1, Sec. 4, Roosevelt Road, Taipei 10617, Taiwan

ARTICLE INFO

Article history:
Available online 26 November 2011

Keywords:
Molecular alignment
Chiral molecules
Molecular beams
Non-adiabatic transitions

ABSTRACT

This theoretical study is complementary to previous experimental work (see D.-C. Che, F. Palazzetti, Y. Okuno, V. Aquilanti, T. Kasai, J. Phys. Chem. A 114 (2010) 3280) on the orientation and rotational state-selection of supersonic molecular beams of the asymmetric-top molecule propylene oxide, both pure and seeded (in He and in Ar) by using an 85-cm length hexapole state-selector. One objective is to obtain an accurate distribution of the rotational states after hexapole selection for the three molecular beams, the most relevant feature consisting in the evaluation of the variation in energy of the manifold of rotational states when an electric field is applied (the Stark forces). Previously, the Stark effect on the effective dipole moment was considered through second order for all rotational states, while in this work the energy derivatives of the rotational states with respect to the applied electric field, are obtained accurately by diagonalizing the very large Stark matrices, whose elements depend on the dipole moment components of the molecule. The Stark energies and the corresponding forces were calculated for values of the electric field between 0 and 80 kV cm^{-1} in steps of 0.5 kV cm^{-1} and then linearly interpolated, covering the whole experimental range of the hexapole. A treatment is given for the intricate pattern of avoided crossings among derivatives of the rotational levels and two limiting cases were considered, corresponding to transitions occurring either adiabatically or diabatically. The two treatments lead to slightly different distributions of the rotational states for the pure and Ar seeded molecular beams, while for the He seeded molecular beam the two distributions are substantially the same. This experimental arrangement is a perspective tool for experiments of photochemistry and scattering of oriented molecules and clusters, and therefore we calculated the orientational distributions in a configuration where a uniform electric field is placed between the hexapole field and the detector.

1. Introduction

The use of an inhomogeneous electric field produced by an electrostatic hexapole was introduced a few decades ago [1,2] in order to provide molecular alignment and to obtain rotational state-selection, and was employed in order to study the dynamics of molecules and clusters of increasing complexity [3–11]. The measurements of the focusing curve of the asymmetric-top molecule propylene oxide [12–21], both as a pure beam and as seeded in He or in Ar, were recently carried out [22] by using a hexapole of 85-cm length. The evaluation of the rotational-state distribution was limited to considering, as usual for the asymmetric-top molecules, only the second-order Stark effect. In order to fully characterize the rotational state distribution of a molecule, which presents a very dense manifold of rotational levels, and whose complexity is higher than most cases previously studied, in the present work we calculate the energy of the rotational states depending on the electric field by diagonalizing the complete Stark matrix (see Section III.B of [10]), whose eigenvalues and their derivatives with respect to the applied field correspond to the Stark energies and the forces locally acting on the molecule flying in the hexapole. Rotational levels and forces as a function of the electric field were obtained between 0 and 80 kV cm^{-1} on a grid of 0.5 kV cm^{-1}. This allows us to calculate the trajectories of the molecules in the experimental apparatus and to discriminate between focusing and defocusing ones. The appearance of a pronounced pattern of avoided crossings which occur between rotational states with the same symmetry, in this case between rotational states with the same quantum number M (the component of the total angular momentum J on a laboratory frame quantization axis; see Section 2.3), lead us to considering two limiting cases, where

☆ Special issue: atomic and molecular clusters.

* Corresponding authors. Tel.: +39 0755855521; fax: +39 0755855606 (F. Palazzetti).
E-mail addresses: kkanda@chem.sci.osaka-u.ac.jp (K. Kanda), fede@dyn.unipg.it (F. Palazzetti).

0301-0104/$ - see front matter © 2011 Elsevier B.V. All rights reserved.
doi:10.1016/j.chemphys.2011.11.020

transitions between states at crossings are treated as occurring either adiabatically or diabatically (see Section 2.6). The algorithm provides ingredients to be extended by including hopping probabilities through e.g. the Landau–Zener formula.

The production of anisotropic orientational distributions for the asymmetric-top molecules by using a hexapole inhomogeneous field combined with a small d.c. homogeneous electric field [23] was also investigated by the calculation of the orientational distribution of the selected states. Curtiss et al. [10] referred to this quantity as the orientation probability distribution function, opdf. For further applications using the brute force field technique on anisotropic orientation of asymmetric-top molecules see in particular papers by Weida and Parmenter [24], Bulthuis et al. [25–27], Loesch and Moeller [28], and Friedrich and Herschbach [29], Lemeshko and Friedrich [30].

This experimental configuration and analysis are expected to provide the starting point for the study of chiral effects in the scattering of oriented molecules, as issued from recent theoretical studies [31–41] which emphasize the role of a well-characterized molecular alignment to favor the manifestation of chiral effects in streams, as relevant not only in photochemistry but also in molecular collisions [42–49].

This paper is organized as follows: in Section 2 we describe the experimental and theoretical background; in Section 3 the results and their discussion are given; conclusions follow in Section 4.

2. Experimental and theoretical background

2.1. Experimental apparatus

Since the experimental apparatus has been described recently [22], here we recall only the features most relevant to this paper. The supersonic molecular beams of both pure propylene oxide, and seeded either in He or in Ar (20% in propylene oxide) were obtained by a source at the stagnation pressure of 0.7 atm (for the pure beam), and of 1.4 atm (for the seeded ones). The molecular beams are produced, analyzed and detected in an experimental setup consisting of a nozzle, a skimmer, a chopper, a collimator, a hexapole, a second collimator and a quadrupole mass-spectrometer.

The velocity distributions were determined by time-of-flight (TOF) measurements for the three supersonic molecular beams. Typically, the pure propylene oxide beam has a velocity at the maximum of the distribution v_M of 670 m/s, and the width at half-maximum of the distribution α_M of 75 m/s. The typical He seeded propylene oxide beam has v_M = 1000 m/s and α_M = 20 m/s, and the Ar seeded propylene oxide beam has v_M = 580 m/s and α_M = 70 m/s. The translational temperature obtained by the velocity distributions are 6 K for the He seeded beam and 20 K for both the pure beam and the Ar seeded beam.

This experimental configuration can be implemented in studies of oriented molecules, crucial in particular regarding the manifestation of chiral effects in molecular flows or in collisions between crossed beams. The additional "orienting" homogeneous electric field is acting in the collision region between the hexapole and the detector (the quadrupole mass spectrometer, see Fig. 1 in [22]). Maintenance of molecular alignment in the passage of the beam from the hexapolar electric field to the orienting field is provided by a guiding field.

2.2. Propylene oxide as an asymmetric-top molecule

Asymmetric-top molecules are characterized by having three unequal components of the moment of inertia along the three axes denoted as *a*, *b*, and *c* [10]. Their structure is intermediate between the two limiting forms of the symmetric-top rotors (two components of the moment of inertia are equal): the prolate-top (cigar-shaped) and the oblate-top (disk-shaped). Rotational states of asymmetric-top molecules are specified by the total angular momentum quantum numbers *J*, and by *M*, its component along a space-fixed quantization axis. The projection of *J* on the molecular symmetry axis, labeled by *K*, which defines the rotational state of symmetric tops, is not a good quantum number for asymmetric tops. However, the combination of *K* at the prolate-top limit, K_{-1}, and the oblate-top limit, K_1, which gives the pseudoquantum number τ, $\tau = K_{-1} - K_1$, allows us to designate the rotational states of the asymmetric-top molecules.

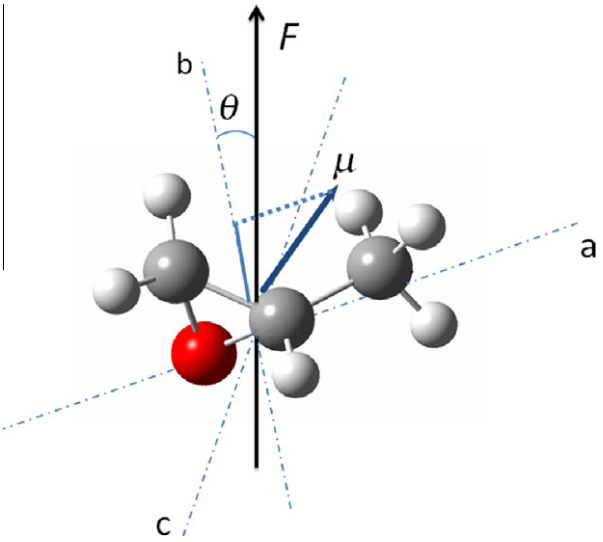

Fig. 1. The figure shows the orientation of the propylene oxide molecule with respect the direction of the orienting field *F*. The three principal axes *a*, *b*, *c*, and the dipole moment μ are reported. The angle θ is given by the intersection between the component of the dipole moment μ along the principal axis *b* and the direction of the orienting field *F*.

Calculations for the rotational energies when electric field is not applied is illustrated in detail in Section III.A of [10]. Here we report the formulas relevant for our treatment.

Asymmetric-top wave functions $A_{J\tau M}$ are given as linear combinations of the symmetric-top wave functions Ψ_{JKM} (see Eqs. (3) and (5) of [10]):

$$A_{J\tau M} = \sum_K a_K^{J\tau M} \Psi_{JKM}. \tag{1}$$

The coefficients $a_K^{J\tau M}$ are eigenvectors obtained from matrix diagonalization (see Eqs. (6a), (6b), and (6c) of [10]), and the corresponding eigenvalues are denoted in [10] as $W_{J\tau M}(k)$, where *k* is the Ray's asymmetry parameter. The rotational energies at *zero field*:

$$W_{J\tau M} = \frac{1}{2}(A + C)J(J + 1) + \frac{1}{2}(A - C)W_{J\tau K}(k), \tag{2}$$

where *A*, *B*, and *C* are the rotational constants, given in [22] for propylene oxide.

2.3. Stark effect

In the free electric field region the $2J + 1$ different spatial orientations of *J* with respect to a laboratory frame quantization axis, denoted as *M*, are degenerate. By applying an electric field this degeneracy persists only for the absolute values of *M*, i.e. $0 \leqslant |M| \leqslant J$. The variation in energy of the rotational states when an electric field is applied provides the Stark force, at times also

considered as an effective dipole moment (see for example Chapter 10 of [50]).

For small molecules and/or low fields the Stark effect is usually considered "first-order" for symmetric-top molecules and "second-order" for asymmetric-top molecules [50]. In this work a more advanced treatment is required to evaluate the effective dependence of the rotational energy levels of propylene oxide on the electric field, in order to calculate the distribution of the population of the rotational states after hexapole state-selection. Field-dependent rotational energy levels $W^M_{J\tau}(E)$ and wave functions $C^M_{J\tau}(E)$ are calculated as eigenvalues and eigenvectors of the Stark matrix $\mathbf{H_S}(E)$ (for the construction of the Stark matrix see Section III.B of [10]). In matrix notation:

$$\mathbf{W_S}(E) = \mathbf{C}\mathbf{H_S}\mathbf{C^T}, \tag{3}$$

where $\mathbf{C}$ is an orthogonal matrix and $\mathbf{C}^T$ its transpose. This large matrix diagonalization is a computational bottleneck in problems of this complexity. The notation $W^M_{J\tau}(E)$ and $C^M_{J\tau}(E)$ corresponds to the correlation with the *zero field* rotational energies $W_{J\tau M}$ (Eq. (2)) and the asymmetric-top wave functions $A_{J\tau M}$, although M is the only good quantum number which survives when the electric field is applied.

The field-dependent wave functions $C_{J\tau M}$ are given by the linear combinations (see Eq. (9) of [10]):

$$C_{J\tau M}(E) = \sum_{J'\tau'} c^{J\tau M}_{J'\tau'}(E) A_{J'\tau' M}, \tag{4}$$

where the elements of $\mathbf{C}$, $c^{J\tau M}_{J'\tau'}(E)$, are the eigenvectors of $\mathbf{H_S}(E)$ in the *zero field* asymmetric-top basis, $A_{J'\tau' M}$.

2.4. Trajectory simulations

The focusing curve is a plot of the dependence of the intensity of the molecular beam on the hexapole voltage. It provides a macroscopic view of the number of molecules (of the beam) which reaches the detector as a function of the applied field. Focusing trajectories are the paths that the molecules follow from the nozzle to the detector, while paths that miss the detector are called non-focusing. The focusing curve is a sum of the contributions to the beam intensity from those molecules which follow focusing trajectories. It depends on the velocity distribution of the molecular beam, on geometrical properties of the experimental apparatus, and on the Stark effect on the rotational levels of the molecules. The simulated focusing curve is calculated by summing the contribution of the individual rotational states, weighted according to their distribution as a function of the rotational temperature, for example assuming equilibrium. The trajectory simulations of hexapole focusing and state-selection of propylene oxide, which have been described in detail previously [22] depart significantly here especially because of the treatment of Stark forces.

The hexapole electric field E is given by (see Eq. (8) of [22]):

$$E = 3V_0 \frac{r^2}{R^3}, \tag{5}$$

where V_0 is the applied voltage, R is the minimum distance between the axis of the hexapole and the surface of the rods of the hexapole, and r is the distance between the axis of the hexapole and the molecule.

The magnitude of the force $\mathfrak{F}(r)$ applied to a molecule in the hexapolar electric field is given by

$$\mathfrak{F}^M_{J\tau}(r) = -\frac{dW^M_{J\tau}(E)}{dr} = -\frac{dW^M_{J\tau}(E)}{dE}\frac{dE}{dr}, \tag{6}$$

(the negative of this force is referred to also as an effective dipole moment). The sign of this force is crucial for the focalization of the trajectories: negative forces (positive Stark effects) lead to focusing trajectories, while positive forces (negative Stark effects) to non focusing trajectories.

Crucial for the accuracy is the direct analytical evaluation of derivatives in Eq. (6). From the definition of the Stark matrix [51], $\frac{dH_S(E)}{dE}$ is given by

$$\frac{dH_S}{dE} = \sum_{g=a,b,c} \mu_g \Phi_{Zg}, \tag{7}$$

where μ_g are the dipole moment components and Φ_{Zg} are the elements of the direction cosine matrix. The derivative of the electric field with respect the distance, $\frac{dE}{dr}$, is:

$$\frac{dE}{dr} = 6V_0 \frac{r}{R^3}. \tag{8}$$

The very demanding calculation of the derivative of the Stark energy with respect the electric field, $\frac{dW^M_{J\tau}(E)}{dE}$, can be performed exactly from these ingredients by applying a theorem in matrix theory, which generalizes the Hellmann–Feynman theorem (see Appendix B of [52] and references therein):

$$\frac{dW^M_{J\tau}}{dE} = \left[\mathbf{C}\frac{d\mathbf{H_S}}{dE}\mathbf{C^T}\right]_{ii}, \tag{9}$$

where $\mathbf{C}$ is the orthogonal matrix of the field-dependent eigenvectors $C_{J\tau M}(E)$ of previous section and the derivatives of the Stark matrix elements with respect to the electric field $\left(\frac{d\mathbf{H_S}}{dE}\right)$ are known analitycally (Eq. (7)). This is seen to be an important improvement with respect to previous work involving no need of numerical differentiation. For example, Curtiss et al. [10] use a low order polynomial interpolation of $W^M_{J\tau}(E)$ on a grid of calculated eigenvalues to compute the derivatives numerically. This for a wide range of E is impractical, in general and particularly troublesome around avoided crossings. Our procedure is accurate, fast and allows a very fine grid even for much larger systems like this one. It is important to note that the same theorem allows the calculation of non adiabatic couplings needed in the following.

Derivatives $\frac{dW^M_{J\tau}(E)}{dE}$ are calculated in the range of electric field between 0 and 80 kv cm^{-1}, in steps of 0.5 kV cm^{-1}, close enough for linear interpolation. The number of rotational states $W^M_{J\tau}(E)$, which govern the trajectories, depends on the rotational temperature of the molecular beam. This parameter is basic for the determination of the distribution of population of the rotational states by the Boltzmann equation. For the pure propylene oxide and the Ar seeded beam, whose rotational temperatures are 30 and 35 K, respectively (see Section 3.1), the simulations were carried out for states up to the maximum value of the quantum number $J = 22$ for a total of 8371, while for the He seeded beam, whose rotational temperature is 10 K (see Section 3.1), the maximum value of J is 12, and the number of rotational states whose trajectories were simulated was 1546.

2.5. The orientational distribution

A homogeneous electric field F placed between the hexapole and the detector permits orientation of the hexapole-selected states, as described for the first time for symmetric-top molecules by Choi and Bernstein [5] (see also [6]). For asymmetric-top molecules, Curtiss et al. calculated the field-dependent orientational distribution $P_{J\tau M}(\cos\theta, E)$ (see Section III.D of [10], where they referred to orientational distribution as "orientational probability distribution function", opdf). Use is made of the following equation (which is equivalent, but simplified with respect to Eq. (14) of [10], observing that one of the sums can be carried out analytically):

$$P_{J\tau M}(\cos\theta, E) = \sum_{J'J''\tau'\tau''K} c^{J\tau M}_{J'\tau'} a^{J'\tau'}_{K} c^{J\tau M}_{J''\tau''} a^{J''\tau''}_{K} \times \frac{(2J'+1)^{\frac{1}{2}}(2J''+1)^{\frac{1}{2}}}{2} \times (-1)^{(M-K)} \times \sum_{n=|J'-J''|}^{J'+J''} (2n+1) \begin{pmatrix} J' & J'' & n \\ M & -M & 0 \end{pmatrix} \times \begin{pmatrix} J' & J'' & n \\ K & -K & 0 \end{pmatrix} P_n(\cos\theta) \quad (10)$$

where the coefficients $c^{J\tau M}_{J'\tau'} a^{J'\tau'}_{K} c^{J\tau M}_{J''\tau''} a^{J''\tau''}_{K}$ are the elements of the eigenvectors (see Sections 2.2 and 2.3), $P_n(\cos\theta)$ is n-th order Legendre polynomials. The angle θ is given by the intersection between the component of the dipole moment of the molecule along the principal axis b and the direction of the orienting electric field F (Fig. 1).

Orientational distributions were calculated in the range of cos θ included between −1 and 1 in steps of 0.1, and for values of the orienting electric field between 0 and 10 kV cm^{-1} in steps of 0.1 kV cm^{-1}.

2.6. Avoided curve crossings and adiabatic passage.

The passage from the hexapolar field $\vec{E}$ to the orienting field $\vec{F}$ must occur in such a way that molecules do not lose their orientation. This adiabatic passage condition is verified when the direction of the electric field $\vec{E}$ during the passage of the molecules changes direction slowly. Accordingly, we study what is the effect on orientation of adding a guiding or buffer field as considered for example in Bulthuis et al. [27] (see also [7,8]).

The pattern of avoided curve crossings occurring between rotational states with the same symmetry, in this case the states $W^M_{J\tau}$ with the same M (see Sections 2.2 and 2.3), the only good quantum number at non zero field. Let two of these states be H_1 and H_2. In the neighborhood of their avoided crossings, trajectories may experience diabatic transitions. The Landau–Zener formula (see e.g. [53]), permits an evaluation of such a transition.

$$P_D = \exp\left(-2\pi \frac{H_{12}^2}{\hbar |v_{LZ}|}\right), \quad (11)$$

where

$$v_{LZ} = \frac{dE}{dt}\frac{d}{dE}|H_{22} - H_{11}| = \frac{dr}{dt}\frac{dE}{dr}\frac{d}{dE}|H_{22} - H_{11}|, \quad (12)$$

and H_{12} is the non-adiabatic coupling matrix elements between H_1 and H_2; $\frac{dr}{dt}$ is the radial velocity, perpendicular to the hexapole axis; $\frac{dE}{dr}$ is given by Eq. (8); finally $\frac{d}{dE}|H_{22} - H_{11}|$ represents the difference in the slope of the states (the forces), which are available, as described in the previous section.It is important to note that the same theorem [52] provides also the explicit way to evaluate H_{12} once known the **C** matrix. Therefore, in case of need in specific applications, one could attribute to trajectories arriving at crossings, probabilities of branching according to an adiabatic ($P_D \approx 0$) or a diabatic ($P_D \approx 1$) behavior.

Under our experimental conditions we estimated that $\frac{dr}{dt} \approx 10$ ms^{-1} $\frac{dE}{dr} \approx 2.5 \cdot 10^9$ V m^{-2}, and $\frac{\partial}{\partial E}|H_{22} - H_{11}|$ is $\approx 10^{-29}$ J mV^{-1}. It follows that for avoided curve crossings separated by an energy gap larger then 10^{-25} J, the probability that diabatic transitions occur can be considered negligible. Instead of accounting for the specific transition probabilities at each crossing, we thought illustrative to confine ourselves here within two limiting cases.

As it has already been explained by Bulthuis et al. (see Section III of [27]), when an adiabatic curve crossing occurs there is frequently a change of the sign of the Stark effect (see Section 2.3), responsible for the focusing or non-focusing nature of the trajectory (see Section 2.4). In the diabatic case, at the avoided crossing point a transition occurs to the adjacent level with no change in the focusing or non-focusing character of the trajectory.

3. Results and discussion

3.1. Stark energies and forces.

In the first columns of Figs. 2 and 3 we report Stark energies $W^M_{J\tau}(E)$ as a function of the hexapolar electric field E for the manifolds of the rotational states for the examples corresponding to $M = 0$ and $M = 3$. In the central columns, blow-ups are shown disentangled according to J values. The corresponding derivatives of the Stark energies with respect to the electric field $\frac{dW^M_{J\tau}(E)}{dE}$ as a function of the electric field are shown in the right columns. The density of the manifold is a visualization of the high number of rotational states involved in the hexapole focusing process. We simulated the trajectories of 8372 states for the pure propylene oxide and the Ar seeded beam (the maximum value of J considered being 22) and 1547 states for the He seeded beam (the maximum value of J considered being 12), whose low rotational temperature and the high velocity emphasize the state-selection.

The representation of the derivatives $\frac{dW^M_{J\tau}(E)}{dE}$ (see the right side of Figs. 2 and 3) exhibits the diversified dependence of the rotational energies on the electric field. Such a dependence must be considered for the discussion of the results, especially when these are compared to those of the previous paper, where we assumed that all the rotational states followed a second-order Stark effect [22]. A high number of values of the electric field within the experimental range (161 values from 0 to 80 kV) and linear interpolation are necessary to represent all rotational states, especially those whose slope (given by the derivatives $\frac{dW^M_{J\tau}(E)}{dE}$) changes abruptly.

3.2. Focusing curves in diabatic and adiabatic limits

Figs. 4–6(a) show the focusing curves for the pure propylene oxide beam, for the one seeded in He and for the one seeded in Ar. Each plot compares experimental focusing curves and those obtained by simulation at the diabatic and adiabatic limits (see Section 2.6).

For the pure propylene oxide molecular beam (Fig. 4(a)) from the time-of-flight measurements reported in the previous paper (see Table 1 of [22]) we determined the peak velocity of the beam, $v_M = 670$ m/s, the width of the velocity distribution at half-maximum, $\alpha_M = 75$ m/s, and the translational temperature $T_{transl} = 20$ K. The rotational temperature T_{rot} was inferred from the best fit of the simulated focusing curve with the experimental one [22]. Both for the diabatic and the adiabatic limits the rotational temperature is 30 K, to be compared to the previous estimate $T_{rot} = 20$ K. The focusing curves obtained by the adiabatic and diabatic limiting cases converge for low and high values of the hexapole voltage, while in the intermediate range differences are pronounced.

For the propylene oxide beam seeded in He (Fig. 5(a)) the velocity distribution determined by time-of-flight measurement in the previous work (see Table 1 of [22]) gave the peak velocity $v_M = 1000$ m/s, the width of the distribution at half-maximum $\alpha_M = 20$ m/s and the translational temperature $T_{transl} = 6$ K. The estimated rotational temperature $T_{rot} = 10$ K is the same for both the diabatic and adiabatic limits, and coincides with the rotational temperature inferred from the simulation curve obtained in the previous work [22]. The simulated focusing curves in the diabatic and adiabatic limits show values very close to each other and provide good fits to the experimental focusing curve.

In Fig. 6a the focusing curves of the propylene oxide seeded in Ar beam are illustrated. As reported in Table 1 of [22], the parameters characterizing the supersonic beam are the peak velocity $v_M = 580$ m/s, the width of the distribution at half-maximum

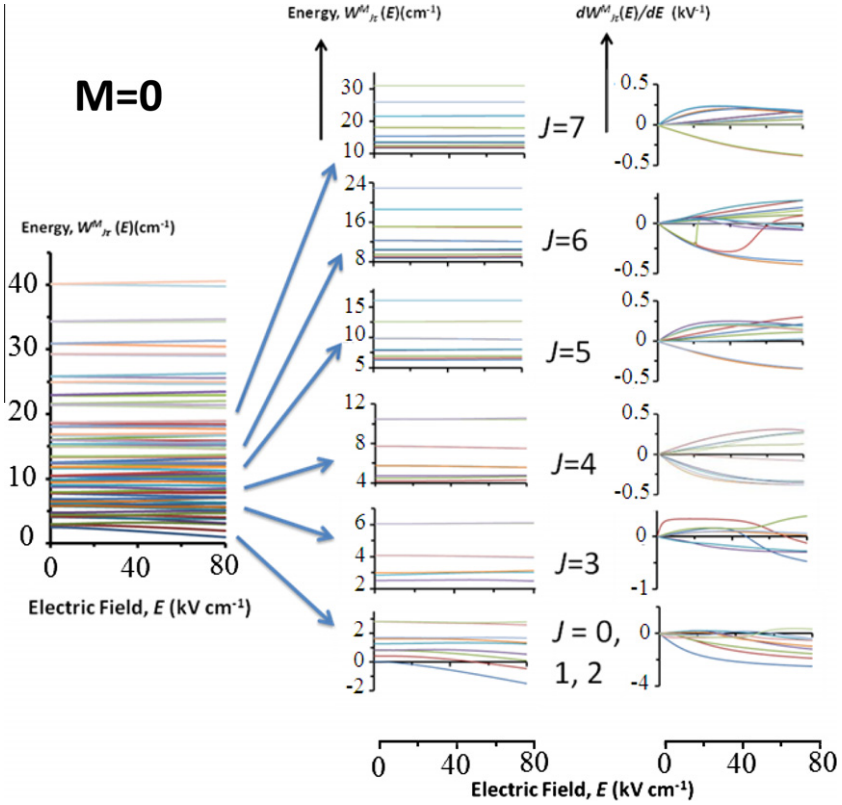

Fig. 2. In the panel in the left side of the figure the energy curves (Stark energy) $W^M_{Jτ}(E)$ depending on the hexapolar electric field, E, are reported for the most important rotational states $W^M_{Jτ}(E)$ for $M = 0$. The central panels show a blow up of the left-side panel for $J = 0, 1, 2$ (first panel from the bottom), $J = 3$ (the second panel), $J = 4$ (the third panel), $J = 5$ (the fourth panel), $J = 6$ (the fifth panel), and $J = 7$ (the last panel). The panels on the right show the derivative $\frac{dW^M_{Jτ}(E)}{dE}$ with respect the electric field. In each panel, the derivatives of the states described in the corresponding central panel are reported.

$\alpha_M = 70$ m/s, and the translational temperature $T_{transl} = 20$ K. The rotational temperature is estimated to be 35 K both in the diabatic and adiabatic limits, to be compared to the previous estimate 20 K [22]. As in the case of the pure propylene oxide beam (Fig. 5(a)), the difference between the simulated focusing curves in the diabatic and adiabatic limiting cases are more pronounced for the intermediate range of hexapole voltages.

To analyze the simulated focusing curves in the diabatic and adiabatic limits (Figs. 4 and 6(a)). For the pure beam and the Ar seeded cases, one has to take into account that the actual behavior may be intermediate. The dense manifold of the rotational states and the complicated molecular trajectories in the hexapole, lead the molecules to experience a wide range of values of the electric field and a diversified behavior at the high number of avoided curve crossings. By contrast, in the He seeded case (Fig. 5) the molecular trajectories are focused in the regions close to the hexapole axis where the electric field is low.

The focusing curves were calculated by summing the contributions of the individual rotational states after hexapole state-selection. The population of the rotational states before the hexapole (in the free-field region) is given by the Boltzmann distribution, at a given rotational temperature, under the assumption of thermal equilibrium (see Section 2.4). The rotational temperature was inferred from the best fit between the simulated focusing curve and the experimental one. As we have mentioned earlier, concerning the simulated focusing curves obtained in the diabatic and adiabatic limiting cases, for the He seeded beam (Fig. 5) there are not appreciable differences between the two simulated focusing curves, while the differences are more prominent for the pure and the Ar seeded beam. We can motivate this behavior as follows: the velocity of the He seeded beam ($v_M = 1000$ m/s) is definetely higher than the pure beam ($v_M = 670$ m/s) and than the Ar seeded beam ($v_M = 580$ m/s), and the velocity distribution at half maximum ($\alpha_M = 20$ m/s) is much narrower than for both the pure beam ($\alpha_M = 75$ m/s) and the Ar seeded beam ($\alpha_M = 70$ m/s). This means that the beam is focused along the axis of the hexapole, where the electric field is lower, thus most of the avoided crossings (see Section 2.6), which occur at higher values of the electric field, are not involved in the overall process. We eventually believe that the remaining differences between experimental and simulated focusing curves, which are noticeable especially in the pure propylene oxide beam and in the Ar seeded propylene oxide beam, could be reduced in case of actual applications of the techniques, by going beyond the two limiting cases (the diabatic and the adiabatic ones, considered here), but through explicit calculation of the probabilities of diabatic transitions at each crossing, as explained in Section 2.6. Actually, the focusing curves for trajectory simulations carried out at the adiabatic and diabatic limits are not to be intended as simulated fits for the curves measured by experiments. The "adiabatic focusing curve" and the "diabatic focusing curve" bracket limits of a range, within which the focusing curve obtained by taking explicitly account of the transition probabilities should be localized. Adjustment of this focusing curve with respect to the experimental one must be carried out to provide fits falling within the width of the error bars: such detailed simulations, involving the calculation of the individual hopping transition probabilities, require implementation of the formulas as demanded in future applications to specific molecules and molecular beams features.

The number of focusing rotational states depends on the rotational temperature of the beam and on its velocity distribution (the rotational states distribution for values of the hexapole voltage 5, 10, and 15 kV, is listed in Supplementary Data). The Ar seeded beam is the one with the highest number of focusing states,

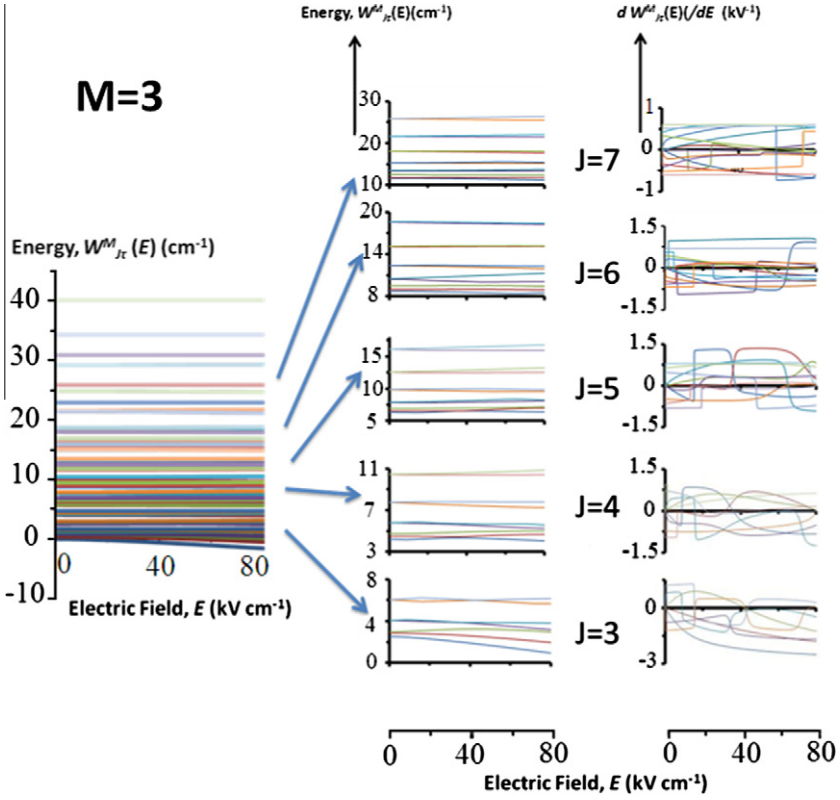

Fig. 3. In the panel in the left side of the figure the energy curves (Stark energy) $W^M_{J\tau}(E)$ depending on the hexapolar electric field, E, are reported for the most important rotational states $W^M_{J\tau}(E)$ for $M = 3$. The central panels show a blow up of the left-side panel for $J = 3$ (first panel from the bottom), $J = 4$ (the second panel), $J = 5$ (the third panel), $J = 6$ (the fourth panel), and $J = 7$ (the last panel). The panels on the right show the derivative $\frac{dW^M_{J\tau}}{dE}$ with respect the electric field. In each panel, the derivatives of the states described in the corresponding central panel are reported.

3117 states at the adiabatic limit and 2484 at the diabatic limit; the pure propylene oxide beam has 2507 focusing states at the adiabatic limit and 1985 at the diabatic limit. Finally the He seeded beam has 364 focusing states at the adiabatic limit and 311 states at the diabatic limit. These differences reflect the fact that certain non-focusing states at the diabatic limit are focusing in a specific range of electric field at the adiabatic limit, or viceversa.

3.3. Orientational distributions

Orientational distributions were calculated for the pure propylene oxide beam and for the beams of propylene oxide seeded in helium and seeded in argon for the adiabatic and diabatic limiting cases, at hexapole voltage of 5, 10 and 15 kV. The total orientational distributions were calculated by summing the contribution of each rotational state, for the three different molecular beams, after rotational state-selection at the three values of the hexapole voltage.

The orientational distributions shown in tridimensional plots in Figs. 4–6(b)–(g) report dependence on the orienting electric field, F (not to be confused with the hexapolar electric field E), and on the angle θ, which is given by the intersection of the component of the dipole moment of the molecule with respect to the principal axis b (the dipole moment lies much closer to this axis) and the direction of the electric field F (see Section 2.4 and Fig. 1). In particular, when the orienting electric field is 0, the orientational distribution is symmetric with respect to cos θ (this angle is not to be confused with the angles Θ and Φ that will be discussed in Sections 3.5 and 3.6).

Figs. 4(b)–(d) show the total orientational distribution for the pure propylene oxide in the adiabatic limit after hexapole state-selection at 5, 10, and 15 kV, when the orienting electric field varies between 0 and 10 kV. As expected orientational distribution at zero orienting field is symmetric with respect to cos θ. For hexapole voltage of 5 kV the orientational distribution is seen to change only slightly with the applied orienting electric field. At 10 kV the orientational distribution has a minimum at cos $\theta = 0$ and reaches the maximum value at cos $\theta = \pm 1$. At 15 kV the orientational distribution has two maxima at cos $\theta \cong \pm 0.5$ and minima at cos $\theta = 0$ and ± 1. The orientational distribution of the pure propylene oxide beam in the diabatic limit (Figs. 4(e)–(g)) is similar to those in Figs. 4(b)–(d).

Figs. 5(b)–(d) show three different orientational distributions depending on the hexapole voltage for the propylene oxide seeded in He beam. At 5 kV (Fig. 5(b)) the maximum orientational distribution is at cos $\theta = 0$ and the minimum at cos $\theta = \pm 1$; at 10 kV the orientational distribution is substantially constant with increasing at cos $\theta = \pm 1$ and a minimum at $\theta = 0$. At 15 kV the trend of the orientational distribution is the opposite than the hexapole voltage set at 5 kV, with a minimum at cos $\theta = 0$ and maximum values at $\theta = \pm 1$. The dependence of the orientational distribution on the orienting electric field F is more pronounced than that shown in Figs. 4(b)–(g). As in the case of the pure propylene oxide beam, the diabatic limit of the He seeded beam (Figs. 5(e)–(g)) gives a similar orientational distribution of the adiabatic limit.

Finally Figs. 6(b)–(d) show the orientational distribution of the propylene oxide beam seeded in Ar (at the adiabatic limiting case) at 5, 10, and 15 kV, respectively. At 5 kV (Fig. 6(b)) there is a strong increase of the orientational distribution close to cos $\theta = \pm 1$, the effect of the orienting electric field is appreciable. At 10 and 15 kV the orientational distribution is smoother than the previous one, with maximum values at $\theta = \pm 0.5$ and minimum values at cos

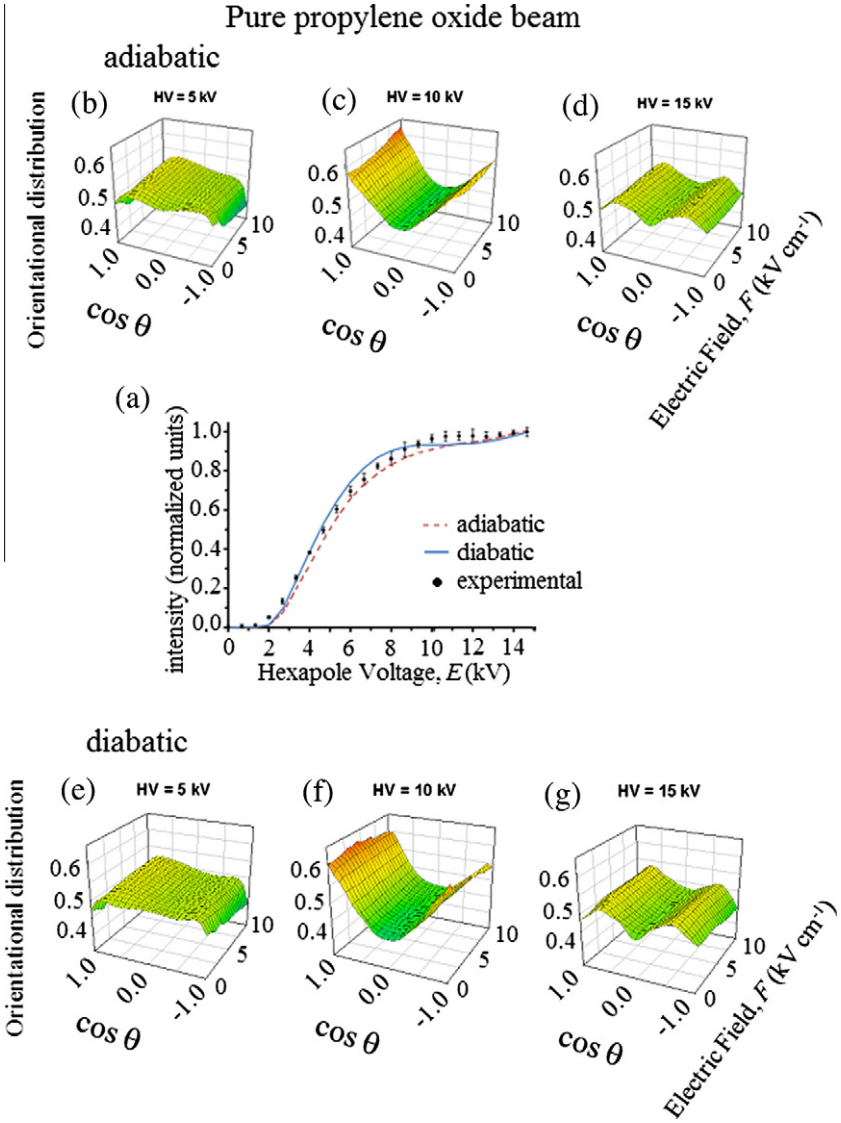

Fig. 4. Focusing curves of the pure propylene oxide supersonic beam (Fig. 4(a)) measured by experiment (dot) and calculated by trajectory simulations at the diabatic (blue continuous line) and adiabatic (red dashed line) limits. Figs. 4(b)–(d) show the orientational distribution in the adiabatic limit for rotational selected states at hexapole voltage of 5, 10, and 15 kV. Figs. 4(e)–(g) illustrate the orientational distribution in the diabatic limit for rotational selected states at hexapole voltage of 5, 10, and 15 kV. (For interpretation of the references to colour in this figure legend, the reader is referred to the web version of this article.)

$\theta = 0, \pm 1$. Also in these cases the dependence of the orientational distribution on the orienting electric field is appreciable. The orientational distributions of the Ar seeded beam in the diabatic limiting case (Figs. 6(e)–(g)) do not show relevant differences.

3.4. J-distributions

Figs. 7(a)–(f) show how the contribution to the simulated focusing curves, for the adiabatic and diabatic limiting cases at the values of hexapole voltage 5, 10, and 15 kV, come from the values of the quantum number J.

Fig. 7a reports the J-distribution for the pure propylene oxide molecular beam. The most important contributions at the hexapole voltage of 5 kV are given by states with J between 5 and 10. At 10 kV states with $J = 5,7$ and 9 are further enhanced, and at 15 kV the states with $J = 5$ become those with the maximum of the distribution. It is interesting to note that the states with $J = 3$ and $J = 6$ do not show enhancement by varying the hexapole voltage and those with $J = 3$ even suffer a decrease. In Fig. 7b the diabatic limiting case for the pure propylene oxide beam is reported. The J-distribution appears similar to that shown in the previous figure.

In Figs. 7(c) and (d) the J-distributions for the He seeded beam in the adiabatic and diabatic limiting cases are shown. In both cases one can observe that at 5 kV the distribution has a smooth trend, the contribution of J increasing from 0 to 4 and then decreasing as J increases.

The J-distributions for the Ar seeded beam at the adiabatic and diabatic limits are reported in Figs. 7(e) and (f). They are similar to those in Figs. 7(a) and (b).

In summary, the diabatic and adiabatic approaches do not lead to large changes in the pictures. Also, the higher velocity distribution for the He seeded beam compared to the pure and the Ar seeded beams is responsible for the focusing of "small" J and for making the J-distribution sharper.

3.5. Angular distributions: Θ angle

In the previous paper [22] we noted that the most of the focusing states had quantum number $M = 0$. In this work we introduce and calculate the angle Θ, as the one which is formed by the intersection between the total angular momentum $\vec{J}$ and the direction of the hexapolar electric field $\vec{E}$. The angle Θ must not be confused

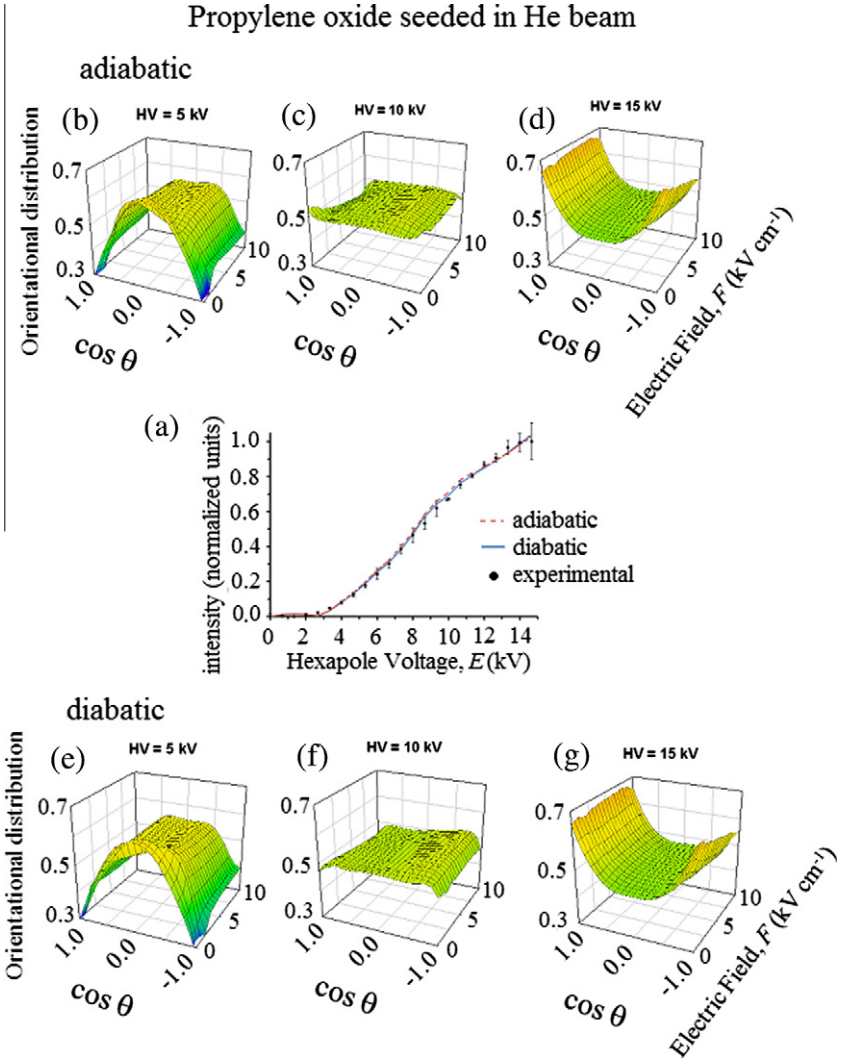

Fig. 5. Focusing curves of the propylene oxide supersonic beam seeded in He (Fig. 5(a)) measured by experiment (dot) and calculated by trajectory simulations at the diabatic (blue continuous line) and adiabatic (red dashed line) limits. Figs. 5(b)–(d) show the orientational distribution in the adiabatic limit for rotational selected states at hexapole voltage of 5, 10, and 15 kV. Figs. 5(e)–(g) illustrate the orientational distribution in the diabatic limit for rotational selected states at hexapole voltage of 5, 10, and 15 kV. (For interpretation of the references to colour in this figure legend, the reader is referred to the web version of this article.)

with θ, which is instead the angle between the component of the dipole moment of the molecule with respect the principal axis b and the direction of the orienting electric field (see Section 2.5 and Fig. 1) and is defined through the semiclassical relationship:

$$\cos\Theta \approx \frac{M}{J+1/2}, \tag{13}$$

which is suggested by the vector model. Therefore, $M = 0$ corresponds to $\cos\Theta = 0$, i.e. to the perpendicular configuration of the total molecular angular momentum with respect to the direction of the hexapolar electric field. In the opposite case, when $M = J$, the value of $\cos\Theta$ depends on J: for high values of J the total angular momentum processes around cones with their axes parallel to the direction of the electric field. Figs. 8(a)–(f) report the distributions of $\cos\Theta$ (as before for the J-distribution) for the three molecular beams at the adiabatic and diabatic limits for values of the hexapole voltage 5, 10 and 15 kV. Distributions are given for $\cos\Theta$ between 0 and 1 for intervals of 0.1. An interesting feature is the negligible presence of focusing states with $\cos\Theta = 0$, corresponding to $M = 0$. Generally, configurations where $\vec{J}$ is nearly perpendicular with respect to $\vec{E}$ are not focused. As we can see by the plots, focusing of states with $\cos\Theta$ close to 0 are more likely in slower beams such as the pure and Ar seeded propylene oxide beams (Fig. 8a-d) and are promoted by increasing the hexapole voltage.

Fig. 8(a), for the pure propylene oxide beam in the adiabatic limit, shows that at low hexapole voltage (5 kV), only states with $\cos\Theta$ greater than 0.4 give an appreciable contribution and most of the distribution is concentrated for values of $\cos\Theta$ from 0.6 to 1. By increasing the hexapole voltage (to 10 kV) also states with $\cos\Theta = 0.2$ contribute, although the effect of the hexapole voltage does not significantly enhance the contribution of states whose value of $\cos\Theta$ is close to 1. Further increases of the hexapole voltage (up to 15 kV) produce variable effects: in some case no changes; in others an increase; in some cases, such as those whose $\cos\Theta$ value is between 0.7 and 0.9, the contribution decreases. For the pure propylene oxide beam in the diabatic limiting case (Fig. 8(b)), the differences are more pronounced at values of $\cos\Theta$ higher than 0.6 and as the hexapole voltage increases.

Fig. 8c presents the distribution of $\cos\Theta$ for the He seeded beam in the adiabatic limit. At 5 kV the only states that are focused are those for which $\cos\Theta$ is greater than 0.5, although the contribution is much lower than that of the pure propylene oxide beam. Increasing of the hexapole voltage makes enhances the contribu-

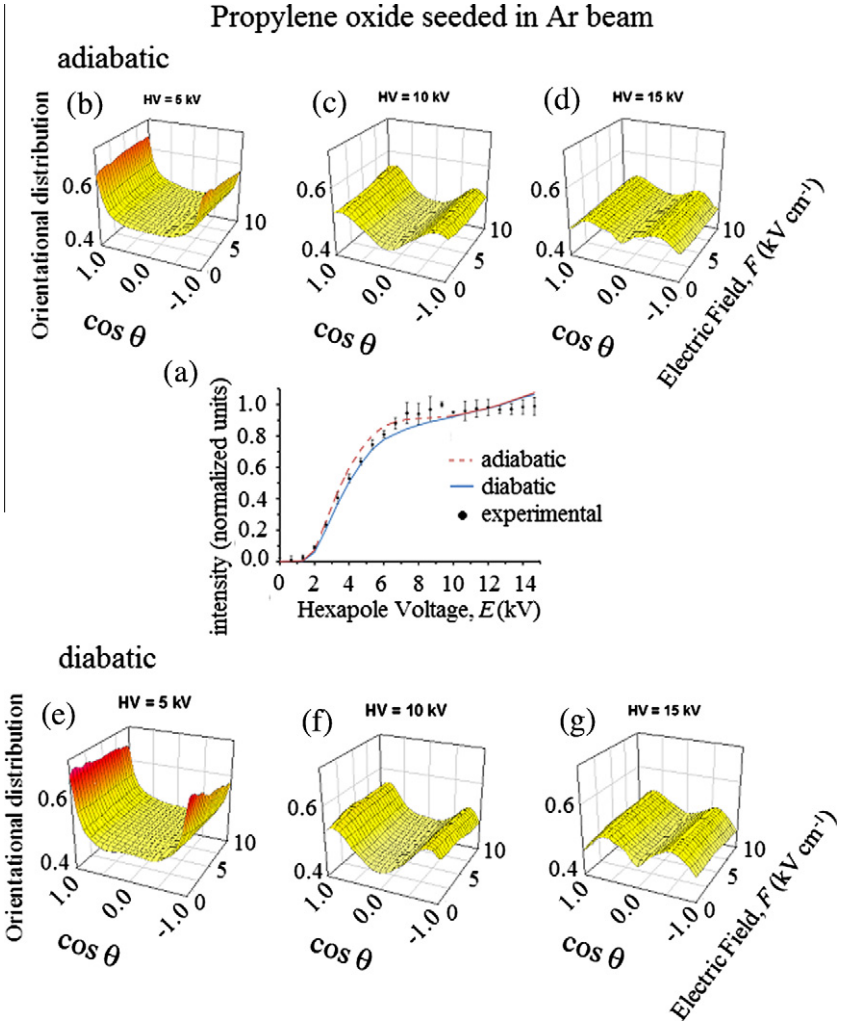

Fig. 6. Focusing curves of the propylene oxide supersonic beam seeded in Ar (Fig. 6(a)) measured by experiment (dot) and calculated by trajectory simulations at the diabatic (blue continuous line) and adiabatic (red dashed line) limits. Figs. 6(b)–(d) show the orientational distribution in the adiabatic limit for rotational selected states at hexapole voltage of 5, 10, and 15 kV. Figs. 6(e)–(g) illustrate the orientational distribution in the diabatic limit for rotational selected states at hexapole voltage of 5, 10, and 15 kV. Fig. 6(f) reports the orientational distribution (diabatic limiting case) at hexapole voltage of 10 kV. Finally in Fig. 6(g) the orientational distribution (adiabatic limiting case) at hexapole voltage of 15 kV is shown. (For interpretation of the references to colour in this figure legend, the reader is referred to the web version of this article.)

tion for states with cos Θ higher than 0.2, even if the strongest effect regards the states with cos Θ greater than 0.5. In Fig. 8(d) the distribution for the diabatic limiting case of the He seeded beam is almost the same than that shown in the previous figure.

The distributions of cos Θ for the Ar seeded beam (see Fig. 8e and f for the adiabatic and diabatic limits) are similar to those of the pure propylene oxide beam even if an appreciable contribution also comes from states with cos $\Theta \approx 0.3$. For states with cos Θ higher than ≈0.8 the effect of the hexapole voltage is negative, the contribution decreasing when the hexapole voltage is greater than 10 kV. In the diabatic limit, for the states with cos Θ between 0.4 and 0.7, the effect is negative when the hexapole voltage increases from 10 to 15 kV, while for states with cos Θ higher than 0.7 there is a negative effect when the hexapole voltage increases from 5 to 10 kV.

3.6. Angular distributions: Φ angle

In the prolate limit, which is the closest to the case of the propylene oxide, the pseudoquantum number τ (see Section 2.2) tends to K, the quantum number which labels the component of the total angular momentum J along the symmetry axis of the molecule. Therefore we can define an angle between $\vec{J}$ and the molecular symmetry axis, as we did before for the angle Θ:

$$\cos\ \Phi \approx \frac{\tau}{J+1/2}, \tag{14}$$

when $\tau \to K$. In Figs. 9(a)–(f) we report the distributions of cos Φ (as previously for J and cos Θ) for the three molecular beams at the adiabatic and diabatic limits. These distributions tell us how the vectors $\vec{J}$ corresponding to the total angular momentum J, arrange with respect to the symmetry axis of the molecule. The distributions are reported for cos $\Phi = 0$, corresponding to the perpendicular arrangement of the direction of the total angular momentum $\vec{J}$ with respect the symmetry axis of the molecule, and for intervals of cos Φ of 0.1 in the range $0 < \cos\Phi < 1$ and $-1 < \cos\Phi < 0$. When $\tau = J$ or $-J$, for high values of J, the total angular momentum becomes almost parallel to the symmetry axis of the molecule.

Figs. 9(a) and (b) report the distributions of cos Φ of the focusing states in the pure propylene oxide beam calculated at the adiabatic and diabatic limits. The plots show a substantial uniformity along the entire range for values of the hexapole voltage of 5 kV. By increasing the hexapole voltage it is interesting to note an increase of the contribution for the states with negative values of cos Φ,

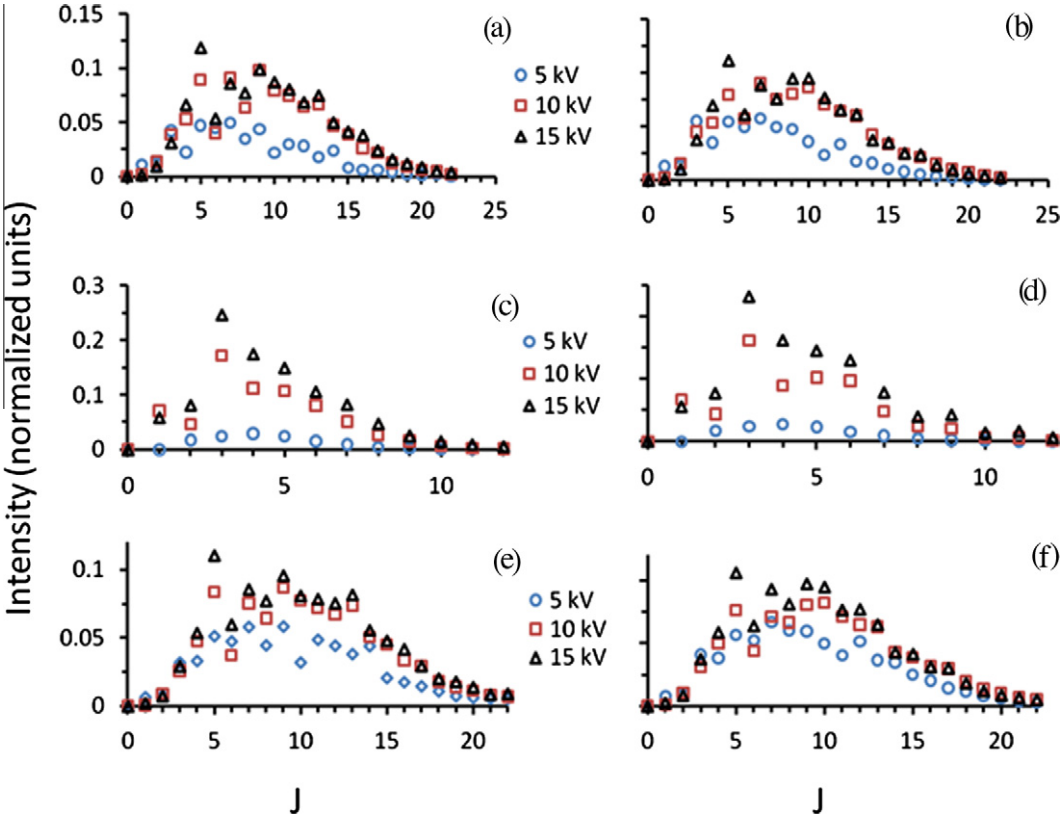

Fig. 7. The distribution of focusing rotational states sorted by the quantum number *J* after hexapolar state selection at hexapole voltage of 5, 10, and 15 kV, is reported for the pure propylene oxide supersonic beam at the adiabatic (Fig. 7(a)) and diabatic (Fig. 7(b)) limits, for the propylene oxide seeded in He supersonic beam at the adiabatic (Fig. 7(c)) and diabatic (Fig. 7(d)) limits, for the propylene oxide seeded in Ar supersonic beam at the adiabatic (Fig. 7(e)) and diabatic (Fig. 7(f)) limits.

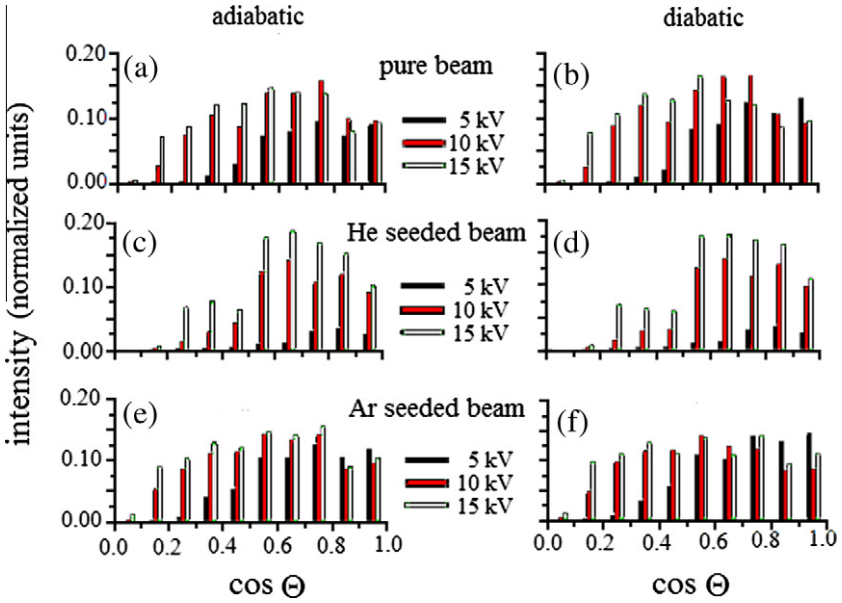

Fig. 8. The distribution of focusing rotational states for cos $\Theta = 0$ and for intervals of cos Θ of 0.1 from 0 (excluded) to 1, after hexapolar state selection at hexapole voltage of 5, 10, and 15 kV, is reported for the pure propylene oxide supersonic beam at the adiabatic (Fig. 8(a)) and diabatic (Fig. 8(b)) limits, for the propylene oxide seeded in He supersonic beam at the adiabatic (Fig. 8(c)) and diabatic (Fig. 8(d)) limits, for the propylene oxide seeded in Ar supersonic beam at the adiabatic (Fig. 8(e)) and diabatic (Fig. 8(f)) limits.

while for the states with positive value of cos Φ the effect is opposite.

Regarding the He seeded (see Figs. 9(c) and (d) for the adiabatic and diabatic limits), contrary to what we have seen in Figs. 9(a) and (b), the distribution of focusing states appears to prevail for those states with positive values of cos Φ and the presence of focusing states with negative cos Φ is negligible at 5 kV, while in general the contribution increases with the hexapole voltage. This

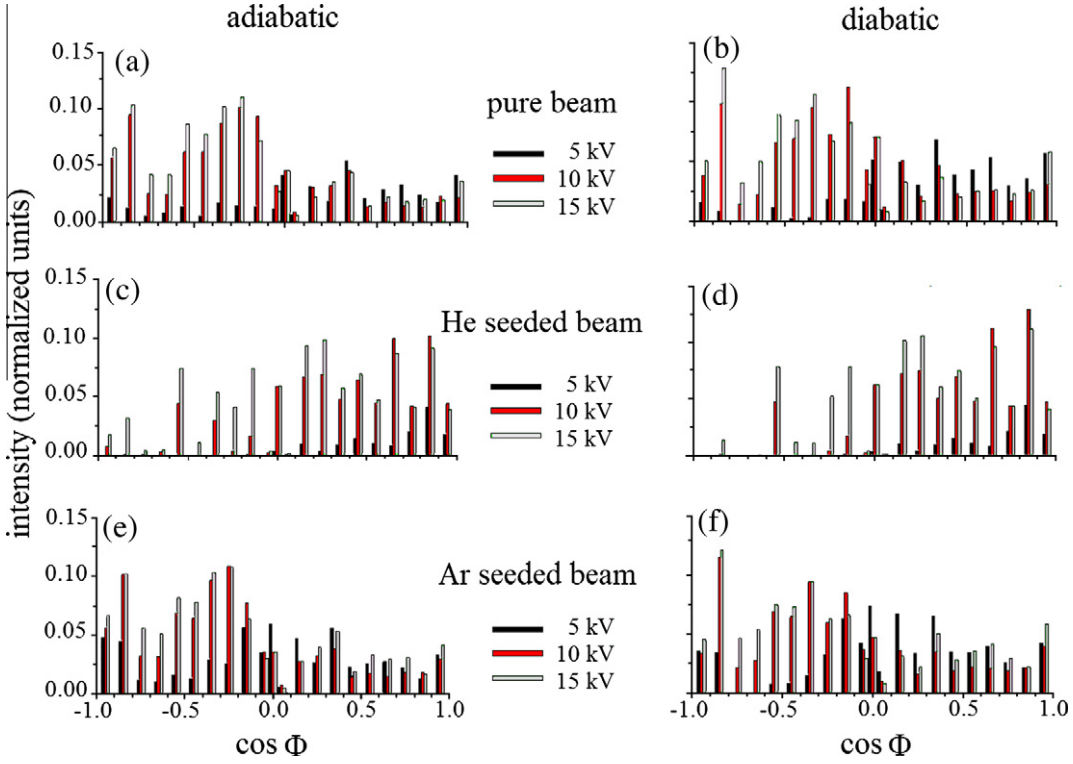

Fig. 9. The distribution of focusing rotational states for cos $\Phi = 0$ and for intervals of cos Φ of 0.1 from 0 (excluded) to 1, after hexapolar state selection at hexapole voltage of 5, 10, and 15 kV, is reported for the pure propylene oxide supersonic beam at the adiabatic (Fig. 9(a)) and diabatic (Fig. 9(b)) limits, for the propylene oxide seeded in He supersonic beam at the adiabatic (Fig. 9(c)) and diabatic (Fig. 9(d)) limits, for the propylene oxide seeded in Ar supersonic beam at the adiabatic (Fig. 9(e)) and diabatic (Fig. 9(f)) limits.

increase is less pronounced at 15 kV for those states with cos Φ higher than ≈0.4 and the contribution becomes lower for cos Φ greater than ≈0.7.

Figs. 9(e) and (f) report the distributions of cos Φ referred to the focusing states of the Ar seeded beam in the adiabatic and diabatic limits. Again, there are no significant differences between the two limits: as we observed for the pure propylene oxide beam the contribution of the states with negative cos Φ is higher for values of the hexapole voltage larger than 5 kV.

4. Summary and concluding remarks.

This work has presented a thorough study of the alignment, orientation and rotational state-selection of the asymmetric-top molecule propylene oxide as a pure supersonic molecular beam, and as seeded either in He (20% in propylene oxide) or in Ar (20% in propylene oxide), reported by Che et al. [22]. In [22] we carried out the experimental measurements of the focusing curves of the three molecular beams and of the corresponding times-of-flight, and provided, by trajectory simulations, results of the distribution of the rotational states after hexapole selection assuming that the rotational energy of the states abide by the second-order Stark effect, i.e. that the energy levels depend on E^2, where E is the hexapolar electric field. Here we have developped and employed a new algorithm which allows us to evaluate the dependence of the rotational energies on the electric field for each state as a function of the hexapolar electric field. The trajectory simulations were carried out in two limiting cases, by assuming that all the avoided crossings, between states with the same symmetry, occur either adiabatically or diabatically, but for specific applications we provided the tools for introducing hopping probabilities as appropriate for each crossing.

The two limits yield overall qualitative agreement but also interesting quantitative differences, both in the calculation of the focusing curves and in the determination of the rotational state-selection. Best agreement was found in the simulation of the focusing curve for the He seeded beam, while for the pure propylene oxide and the Ar seeded beam the differences are more evident. This may be due to the fact that the trajectories of the propylene oxide, when seeded in He, are mostly focused along the axis of the hexapole where the hexapolar electric field is weaker, so that most of the avoided crossings are energetically inaccessible. For the pure propylene oxide beam and for the beam seeded in Ar, the profile is wider and the molecules experience higher electric fields. The rotational temperatures inferred by the focusing curves gave similar result for the diabatic and adiabatic limiting cases: for the pure propylene oxide beam it is 30 K, for the He seeded beam it is 10 K and for the Ar seeded beam it is 35 K. In the previous work the rotational temperatures were 20 K for the pure propylene oxide and Ar seeded beams, and 10 K for the He seeded beam. In general, the differences between the two limiting cases are an indication that for an accurate analysis one should introduce explicitly the transition probabilities at most relevant crossings, and tools for implementing these are described in Section 2.6. The orientational distributions were calculated for the three molecular beams in the adiabatic and diabatic limits for the experimental configuration where an orienting field F is placed between the hexapole and the detector.

The orienting electric field was varied in the interval from 0 to 10 kV cm^{-1}, for the three molecular beams in the diabatic and adiabatic limits, and at values of hexapole voltage of 5, 10, and 15 kV. The results obtained in the adiabatic and diabatic limiting cases are substantially similar.

The number of the focusing states is higher in the Ar seeded beam and in the pure propylene oxide beam, while in the He seeded beam the state-selection is sharper. One reason for this behavior is due to the molecular velocity, being the focusing more efficient for slower beams. Also, the rotational temperature plays a role in the population of the rotational levels. Thus as expected the Ar seeded beam is the one with the highest number of focusing states, while the He seeded beam is the more selective. The discrepancy between the focusing states in the diabatic and adiabatic limits reflects the change in slope of the curves at adiabatic crossings, corresponding to the focusing or non-focusing nature of the states.

The distribution of the quantum number J, and of the angles Θ and Φ were calculated for the three molecular beams in the adiabatic and diabatic limits, in order to visualize the molecular behavior. For the pure propylene oxide beam the distribution is concentrated among the states with J between 5 and 10. Increasing the hexapole voltage the distribution becomes sharper. At 15 kV the states with $J = 5$ are those with the highest distribution. Increase of the hexapole voltage produces different effects on the states, for example the states with $J = 6$ do not show enhancements, while states with $J = 3$ decrease for high values of the hexapole voltage. The J-distribution for Ar seeded beams is similar to that for the pure propylene oxide beam, while for the He seeded beam the maximum of the contribution occurs for $J = 3$. It is interesting to note how in the He seeded beam the distribution of J is smoother.

The distributions of cos Θ and cos Φ give us information about the motion of the focusing states. The plots show that molecules with $M = 0$, namely with the total angular momentum perpendicular with respect to the direction of the hexapolar electric field $\vec{E}$, are not focused. The beam velocity plays an important role in the state selection: in the He seeded beam (high beam velocity) at low hexapole voltage only the states with cos Θ close to 1 (the states whose total angular momentum is almost parallel to the hexapolar electric field direction) are focusing. A general increase of the contribution occurs for all states, even if those states with cos Θ close to 0 do not show enhancement. For the low velocity pure propylene oxide beam and Ar seeded beam, the maximum of the contribution depends on the hexapole voltage, and moves from cos $\Theta = 1$ to lower values as the voltage increases.

To appreciate the role of the dependence on cos Φ, since propylene oxide has an asymmetry Ray's parameter of 0.87 [22], so it is a nearly prolate top, and the pseudoquantum number τ can be assimilated to the quantum number K. We can distinguish two cases based on the beam velocity. For the pure propylene oxide and Ar seeded beam an increase of the hexapole voltage moves the maximum of the distribution to negative values of τ, while the opposite effect occurs for the He seeded beam.

In conclusion, we remark that for molecules such as propylene oxide, for which the manifold of rotational states is very dense, it is not possible to make a prediction of the Stark effect of the rotational levels on the basis of the asymmetry, but an accurate treatment is necessary. The treatment of the pattern of the avoided crossings is crucial. The diabatic and adiabatic limits lead to slightly different results and the difference are larger for slow beams. The corresponding focusing curves bracket the limits of a range, in which the focusing curve obtained by taking into account of the hopping transition probabilities should be localized. Such a kind of detailed calculations can be carried out when needed and recipes are given for such applications. Since both the beam velocity and the hexapole voltage play a basic role in the state-selection, changing these parameters modulates the spatial arrangement of the focused molecules. The asymmetric orientational distribution confirms the suitability of the hexapole technique for propylene oxide in experiments of photochemistry and scattering. This paper also provides theoretical and computational tools for extending these techniques to molecules of relevant complexity.

Acknowledgments

Federico Palazzetti expresses his special thanks to the Global COE (center of excellence) Program for "Global Education and Research Center for Bio-Environmental Chemistry" of Osaka University. The Japanese Ministry of Education, Science, and Culture is gratefully acknowledged for a Grant Aid for Scientific Research (Nos. 20350006 and 21550013) in support of this work. Research in Perugia was supported by MIUR (the Italian Ministry for Research, University and Education), Fondazione Cassa di Risparmio di Perugia, and ASI (the Italian Space Agency).

Appendix A. Supplementary data

Supplementary data associated with this article can be found, in the online version, at doi:10.1016/j.chemphys.2011.11.020.

References

[1] P.R. Brooks, E.M. Jones, K. Smith, J. Chem. Phys. 51 (1969) 3073. and references therein.
[2] H.K. Kramer, R.B. Bernstein, J. Chem. Phys. 742 (1965) 767.
[3] P.R. Brooks, J. Chem. Phys. 130 (2009) 151102.
[4] P.R. Brooks, J. Phys. Chem. A 113 (2009) 14296.
[5] S.E. Choi, R.B. Bernstein, J. Chem. Phys. 85 (1986) 150.
[6] T.D. Hain, M.A. Weibel, K.M. Backstrand, T.J. Curtiss, J. Phys. Chem. A 101 (1997) 7674.
[7] H. Ohoyama, T. Ogawa, T. Kasai, J. Chem. Phys. 99 (1995) 13606.
[8] M. Hashinokuchi, D.-C. Che, D. Watanabe, T. Fukuyama, I. Koyano, I. Shimizu, A. Woelke, T. Kasai, Phys. Chem. Chem. Phys. 5 (2003) 3911.
[9] E.M. Jones, P.R. Brooks, J. Chem. Phys. 53 (1970) 55.
[10] T.D. Hain, R.M. Moision, T.J. Curtiss, J. Chem. Phys. 111 (1999) 6797.
[11] R.W. Anderson, J. Phys. Chem. 1997 (2010) 3280664.
[12] J.D. Swalen, D.R. Herschbach, J. Chem. Phys. 27 (1957) 100.
[13] D.R. Herschbach, J.D. Swalen, J. Chem. Phys. 29 (1958) 761.
[14] F. Dubnikova, A. Lifshitz, J. Phys. Chem. A 104 (2000) 4489.
[15] K. Frimand, K. Jalkanen, J. Chem. Phys. 279 (2002) 161.
[16] M.C. Tam, N.J. Russ, T.D. Crawford, J. Chem. Phys. 121 (2004) 3550.
[17] H. Zhang, J. Ming-Xing, X.X. Song, C.X. Hui, D.D. Jun, Front. Phys. China 3 (2006) 275.
[18] A. Lifshitz, C. Tamburu, J. Phys. Chem. 98 (1994) 1161.
[19] X. Xu, Z. Hu, M.X. Jin, H. Liu, D. Ding, J. Mol. Struct. TEOCHEM 638 (2006) 215.
[20] G. Zhang, A. Yin, Int. J. Quantum Chem. 109 (2009) 920.
[21] Z. Su, Y. Xu, Angew. Chem. 46 (2007) 6163.
[22] D.-C. Che, F. Palazzetti, Y. Okuno, V. Aquilanti, T. Kasai, J. Phys. Chem. A 114 (2010) 3280.
[23] V. Aquilanti, M. Bartolomei, F. Pirani, D. Cappelletti, F. Vecchiocattivi, Y. Shimizu, T. Kasai, Phys. Chem. Chem. Phys. 7 (2005) 291.
[24] M.J. Weida, C.S. Parmenter, J. Phys. Chem. A 101 (1997) 9594.
[25] J. Bulthuis, J. Moeller, H.J. Loesch, J. Phys. Chem. A 101 (1997) 7684.
[26] W. Kong, J. Bulthuis, J. Phys. Chem. A 104 (2000) 1055.
[27] J. Bulthuis, J.B. Milan, M.H.M. Janssen, S. Stolte, J. Chem. Phys. 94 (1991) 7181.
[28] H.J. Loesch, A. Remscheid, J. Chem. Phys. 93 (1990) 4779.
[29] B. Friedrich, D.R. Herschbach, Nature 353 (1991) 412.
[30] M. Lemeshko, B. Friedrich, J. Chem. Phys. 129 (2008) 024301.
[31] A. Busalla, K. Blum, T. Beyer, B.M. Nestmann, J. Phys. B 32 (1999) 791.
[32] M. Musigmann, A. Busalla, K. Blum, D.G. Thompson, J. Phys. B 32 (1999) 4117.
[33] A. Busalla, K. Blum, D.G. Thompson, Phys. Rev. Lett. 83 (1999) 1562.
[34] M. Musigmann, A. Busalla, K. Blum, D.G. Thompson, J. Phys. B 34 (2001) L79.
[35] H.-N. Lee, T.-M. Su, I. Chao, J. Phys. Chem. A 108 (2004) 2567.
[36] V. Aquilanti, G.S. Maciel, Origins Life Evol. Biosph. 36 (2006) 435.
[37] V. Aquilanti, D. Ascenzi, D. Cappelletti, F. Pirani, Nature 371 (1994) 399.
[38] V. Aquilanti, G. Grossi, A. Lombardi, G.S. Maciel, F. Palazzetti, Phys. Scripta 78 (2008) 058119.
[39] A. Lombardi, F. Palazzetti, G.S. Maciel, V. Aquilanti, M.B. Sevryuk, Int. J. Quantum Chem. 111 (2011) 1651.
[40] V. Aquilanti, G. Grossi, A. Lombardi, G.S. Maciel, F. Palazzetti, Rendiconti Lincei 22 (2011) 125.
[41] A. Lombardi, G.S. Maciel, F. Palazzetti, G. Grossi, V. Aquilanti, J. Vac. Soc. Jpn. 53 (2010) 645.
[42] S. Turchini, N. Zema, G. Contini, G. Alberti, M. Alagia, S. Stranges, G. Fronzoni, M. Stener, P. Decleva, T. Prosperi, Phys. Rev. A 70 (2004) 014205.
[43] S. Stranges, S. Turchini, M. Alagia, G.A.G. Contini, P. Decleva, G. Fronzoni, M. Stener, N. Zema, T. Prosperi, J. Chem. Phys. 122 (2005) 244303.

[44] S. Portmann, A. Inauen, H.P. Luethi, S. Leutwyler, J. Chem. Phys. 113 (2000) 9577.
[45] A. Zehnacker, M.A. Suhm, Angew. Chem. 47 (2008) 6970.
[46] M.N. Piancastelli, T. Lischke, G. Pruemper, X.J. Liu, H. Fukuzawa, M. Hoshino, T. Tanaka, H. Tanaka, J. Harries, Y. Tamenori, Z. Bao, O. Travnikova, D. CTolin, K. Ueda, J. Electron Spectrosc. Relat. Phenom. 156 (2007) 259.
[47] G. Alberti, S. Turchini, G. Contini, N. Zema, T. Prosperi, S. Stranges, V. Feyer, P. Bolognesi, L. Avaldi, Phys. Scripta 78 (2008) 058120.
[48] H.-N. Lee, L.C. Chang, T.-M. Su, Chem. Phys. Lett. 507 (2011) 63.
[49] O. Ortega, A. Canillas, J. Crusats, Z. El-Hachemi, J. Llorens, A. Sorrenti, J.M. Ribò, Isr. J. Chem. 51 (2011) 1007.
[50] C.H. Townes, A.L. Schawlow, Microwave Spectroscopy, Dover Publications, Inc., New York, 1975. Chapters 4 and 10.
[51] P.C. Cross, R.M. Hainer, G.W. King, J. Chem. Phys. 12 (1944) 210.
[52] V. Aquilanti, S. Cavalli, M.B. Sevryuk, J. Math. Phys. 35 (1994) 536.
[53] A. Schwettmann, J. Franklin, K.R. Oversreet, J.P. Shaffer, J. Chem. Phys. 123 (2005) 194305.